IEEE Access
Multidisciplinary | Rapid Review | Open Access Journal

Received March 2, 2021, accepted March 16, 2021, date of publication March 24, 2021, date of current version April 6, 2021.

Digital Object Identifier 10.1109/ACCESS.2021.3068520

Light-Field-Assisted Phase Unwrapping of Fringe Projection Profilometry

ZIWEI WANG[1], YANG YANG[1], XIAOLI LIU[1], YUPEI MIAO[1], QUANYAO HOU[1], YONGKAI YIN[2], ZEWEI CAI[1], QIJIAN TANG[1], AND XIANG PENG[1]

[1]Key Laboratory of Optoelectronic Devices and Systems of Ministry of Education and Guangdong Province, College of Physics and Optoelectronic Engineering, Shenzhen University, Shenzhen 518060, China
[2]School of Information Science and Engineering, Shandong University, Qingdao 266237, China

Corresponding author: Qijian Tang (ytqjtang@163.com)

This work was supported in part by the National Natural Science Foundation of China (NSFC) under Grant 61875137, in part by the Fundamental Research Project of Shenzhen Municipality under Grant JCYJ20190808153201654, in part by the Sino-German Cooperation Group under Grant GZ1391 and Grant M0044, and in part by the Key Laboratory of Intelligent Optical Metrology and Sensing of Shenzhen under Grant ZDSYS20200107103001793.

ABSTRACT A phase unwrapping algorithm assisted by light field without additional time coding is proposed, which can be used in various aspects of optical imaging and metrology. The phase consistency between the light field and the industrial camera is the sticking point to convert the angular resolution of the light field into the order of phase. By virtue of the angle information recorded by the light field, the correct order can be uniquely determined from several candidate orders without confusion in the measurement volume. The mandatory requirements for system fixation and pre-calibration and the connection between the light field and industrial camera are prerequisites for order uniqueness. The mapping relationship established by the phase implies coordinate conversion, lens distortion and other factors, thus providing a high degree of stability for the transmission of phase order information. The achieved results demonstrate that our method is robust and can be taken as an effective tool for means of phase unwrapping.

INDEX TERMS FPP, phase unwrapping, structured light, light field.

I. INTRODUCTION

Fringe projection profilometry (FPP) is used extensively in optical three-dimensional (3D) measurements credit to its high resolution, precision, and speed. FPP usually projects sinusoidal fringes to obtain the information modulated by the surface of the object [1]–[5], the phase distribution is wrapped to the principal value ranging between $-\pi$ and π. Consequently, the phase unwrapping must be carried out to obtain a continuous phase map. Commonly used phase unwrapping algorithms can be divided into two categories, spatial phase unwrapping [6]–[9] and temporal phase unwrapping [10]–[13]. Temporal phase unwrapping needs to project more encoded information as a time series signal, which requires more image acquisition time, and therefore reduces the measurement speed [11], [14]–[16]. With the help of multi-view geometric constraints, another type of absolute phase unwrapping method has been developed to avoid the situation of acquiring or embedding additional encoded information. Various constraints, such as measurement volume, phase value, phase monotonicity, epipolar geometry, and trifocal tensor can be used to find corresponding points from different angles to determine the correct unwrapped phase [17]–[19].

In our view, light field can provide multi-viewpoint constraint for phase unwrapping, which can record the position and direction information of the light at the same time to realize multi-viewpoint imaging [20], [21]. In order to distinguish the direction of light, usually a camera array [22] or a single camera with an optical modulation module, such as a microlens array, mask, etc., is used [23]. Usually display or blur is used to estimate the depth of light field data, but both of these techniques use passive illumination. The former matches between multi-viewpoint images to calculate the disparity map, while the latter focuses on different depths to obtain the focus stack, then estimates the blur kernel and degree of focus [24]–[30]. The ascendancy of passive illumination is that it can realize depth perception

The associate editor coordinating the review of this manuscript and approving it for publication was Hossein Rahmani.

without any auxiliary equipment, but passive illumination lacks robustness, which seriously affects the quality of depth estimation, and cannot handle complex scenes. Structured light active illumination offers intensity-insensitive encoded phase information to accurately construct matching features, greatly enhances robustness and accuracy, and can easily solve the above shortcomings. In our previous work, Cai *et al.* combined structured light and light field to develop a structured light field, which encodes light field information and applies it to unwrap the phase in light field [31]. Thereby, multi-view depth measurement and 3D reconstruction [32], [33] and unfocused plenoptic camera depth measurement relationship has been carried out [34].

Cai determined the phase order by comparing the phase consistency of the spatial candidate points in the light field. Due to the tradeoff between the spatial resolution and the angular resolution of the plenoptic camera, too much spatial resolution is sacrificed in order to obtain the angular resolution, despite the huge amount of sampled data. The loss of spatial resolution in the process of finding spatial candidate points through angular resolution is a fundamental disadvantage. The method of ray calibration is used to reconstruct the space target object, that is, one pixel is mapped to a ray in the space, but in fact, this pixel is imaged by a cluster of rays in space. The imaging of pixels by non-single ray means that the spatial resolution has a great negative impact on the reconstruction accuracy of the ray calibration method. Therefore, using angular resolution for phase unwrapping, without sacrificing spatial resolution, is the intention of our work. This method of obtaining the structured light field's fast phase unwrapping characteristics and the FPP system's high-resolution features at the same time will be a major improvement in the phase unwrapping method. For this reason, in this paper, the phase unwrapping method in the FPP system assisted by light field is presented to realize phase unwrapping of the wrapped phase of an absolute isolated complex object. The FPP system consists of a digital projector and an industrial camera, and the light field imaging device is a plenoptic camera. Different from [31], our method is to compare the phase consistency between the light field and the FPP system, in which the light field is only used to assist in the phase expansion, and the lower light field spatial resolution does not harm the resolution of the FPP system. Phase expansion is carried out by using the characteristics of the multi-view angle of the light field, that is, no extra time series pattern is required to be projected, and the resolution is not limited by the number of microlenses. The focus of this work is to construct a spatial mapping relationship between a light field camera and the FPP system, so as to transfer the orders information obtained through the angle resolution of the light field to the FPP system. This method of using the phase value generated by the sinusoidal structured light projection as the mark point to establish the mapping relationship is a more efficient method than the traditional target feature point. Experiments proved that our mapping is effective and stable, the light field system can provide accurate phase orders for the FPP system, and that the phase unwrapping can proceed smoothly while ensuring the resolution of the FPP system. TFThis is a high-speed and accurate phase unwrapping method with high reconstruction accuracy and phase unwrapping efficiency.

II. METHODS

A. BASIC PRINCIPLE OF FPP AND RECONSTRUCTION

Traditionally, the absolute phase has been assessed by projecting sinusoidal fringes, as shown in Eq.1. Generally, in the N-step phase shift algorithm, the fringe image of the measured object under the fringe projection of the projector can be captured by a conventional camera with its intensity.

$$I_n(x, y) = A(x, y) + B(x, y)cos[\phi(x, y) + \delta_n] \tag{1}$$

where (x, y) represents the image pixel coordinates, A and B are the background light intensity and modulation intensity, respectively, ϕ is the modulation phase, $\delta_n = \frac{2n\pi}{N}$ is the phase shift, n represents the n-th phase shift, and N is the number of phase shift steps. Through multi-step phase shift we can calculate the modulation phase, as in Eq.2.

$$\phi_w(x, y) = arctan\frac{-\sum_{n=1}^{N} I_n(x, y)\sin\delta_n}{\sum_{n=1}^{N} I_n(x, y)\cos\delta_n} \tag{2}$$

Since the arctangent function only ranges from $-\pi$ to π, the phase value provided from Eq.2 will have 2π phase discontinuities. To obtain continuous phase distribution, phase unwrapping must be carried out. We fit the corresponding relationship between the camera coordinate system and their unwrapped phase by using the mapping polynomial, which is expressed by the following formula [35].

$$\begin{cases} X_c = \dfrac{1}{\sum_{n=1}^{N} a_n \phi_c^n(x,y)} \\ Y_c = \dfrac{1}{\sum_{n=1}^{N} b_n \phi_c^n(x,y)} \\ Z_c = \dfrac{1}{\sum_{n=1}^{N} c_n \phi_c^n(x,y)} \end{cases} \tag{3}$$

where X_c,Y_c and Z_c represents the position in the camera coordinate system, $\phi_c(x, y)$ represents the unwrapped phase of pixel in the camera imaging plane and a_n, b_n and c_n represent the corresponding fitting coefficients. The fitting order N of the polynomial is determined by the lens distortion and the nonlinear epipolar. Only the distortion of the lens exists in the calculation of X_c to make it is a 7th order polynomial, but the Y_c and Z_c are determined by X_c and the epipolar line, and the epipolar line can be approximated as a 5th order polynomial curve, so the order of Y_c and Z_c is 35th order.

B. LIGHT FIELD COORDINATE

We created the light field coordinate system O-uvD as shown in Fig.1, which is consistent with the Euclidean coordinate

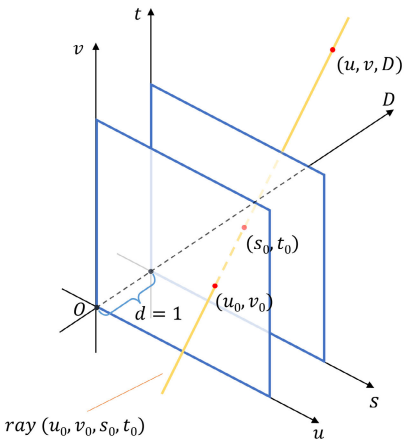

FIGURE 1. Five-dimensional light field coordinate system.

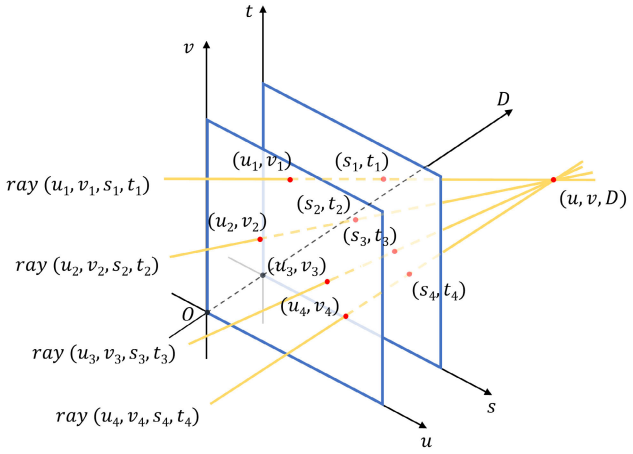

FIGURE 2. Light beam in five-dimensional light field coordinate system.

system. The coordinate axis O-D is perpendicular to axis O-u and axis O-v, and intersects the plane (u, v) at the coordinate origin($u = 0, v = 0, D = 0$). In this coordinate system, the coordinates of a space point can be expressed as (u, v, D) which projected onto the plane (u, v) along the D axis, and the axis O-D represents the absolute depth in the light field. The two-plane method is usually used to represent rays, with the plane (u, v) representing the position, and the plane (s, t) representing the direction. The plane (u, v) and O-uv in the light field coordinate system are superimposed together to describe all the rays in the light field. The plane (u, v) is parallel to the plane (s, t), while the coordinate axis O-D is perpendicular to them and intersects plane (u, v) at the coordinate origin ($u = 0, v = 0, D = 0$). The distance between the plane (u, v) and (s, t) is 1, just so that the difference between the corresponding coordinate values on the plane (s, t) and (u, v) is equal to the tangent of the straight-line angle. A point on a line in a specified direction can be represented by a five-dimensional coordinate (u, v, s, t, D), in which (s, t) are the coordinates difference projected onto the plane (s, t) and (u, v) along the ray. The equation of the ray where the point located is described by $\frac{u-u_0}{s} = \frac{v-v_0}{t}$, and (s, t) is the direction vector of the line. When the ray spreads distance D from the plane (u, v), let the linear equation be equal to the absolute depth $D(\frac{u-u_0}{s} = \frac{v-v_0}{t} = D)$, then the coordinate of the point(u, v, D) after ray spreading can be obtained.

$$\begin{cases} u = u_0 + sD \\ v = v_0 + tD \end{cases} \tag{4}$$

The position of the point (u, v, D) after the ray spreads can be determined by Eq.4. The difference of the point in the (u, v) coordinates after the ray spreading is related to the spreading distance D and proportional to the light propagation direction (s, t). Eq.4 can also represent the difference in (u, v) coordinates at different directions (s, t) when the point light source emits light in different directions. As shown in the Fig.2, light rays passing through the same point in different directions are represented by different coordinates (s, t), and the light beam is composed of them.

For the light ray emitted from a point (u, v, D) at a distance of D from the plane (u, v), in different ray directions (s, t), the difference in (u, v) coordinate with the central viewing angle $(s = 0, t = 0)$ is only related to the direction (s, t) and the depth D. When the depth D of the light source changes, the changed depth D can be perceived through the (u, v) coordinate changes under different viewing angles (s, t). The same amount of depth D corresponds to the same object point under different ray directions, so precise D can be determined by the following an overdetermined equation.

$$\begin{cases} (u, v) = (u_1, v_1) + (s_1, t_1)D \\ (u, v) = (u_2, v_2) + (s_2, t_2)D \\ (u, v) = (u_3, v_3) + (s_3, t_3)D \\ \quad\vdots \qquad\qquad\quad \vdots \\ (u, v) = (u_n, v_n) + (s_n, t_n)D \end{cases} \tag{5}$$

(u, v, D) is the coordinate of the object point, $(s_1, t_1) \cdots (s_n, t_n)$ represent different ray directions, and $(u_1, v_1) \cdots (u_n, v_n)$ are the coordinates of the object point projected onto the (u, v) plane along the ray. The least square solution of this equation is the absolute depth D corresponding to the precise depth of the object point.

C. DEPTH CONSTRAINT AND PHASE UNWRAPPING

The light field coordinate system can be transformed to the FPP coordinate system (world coordinate system) with the principal point of the industrial camera as the origin through coordinate transformation, which is essentially determined by the optical axis of the industrial camera and the light field.

$$\begin{bmatrix} u \\ v \\ D \end{bmatrix} = \begin{bmatrix} r_{11} & r_{12} & r_{13} \\ r_{12} & r_{22} & r_{23} \\ r_{31} & r_{32} & r_{33} \end{bmatrix} \begin{bmatrix} X_c \\ Y_c \\ Z_c \end{bmatrix} + \begin{bmatrix} t_1 \\ t_2 \\ t_3 \end{bmatrix} \tag{6}$$

Eq.6 represents the above transformation, (u, v) on the imaging surface of the light field in pixels, and (X_c, Y_c, Z_c) and

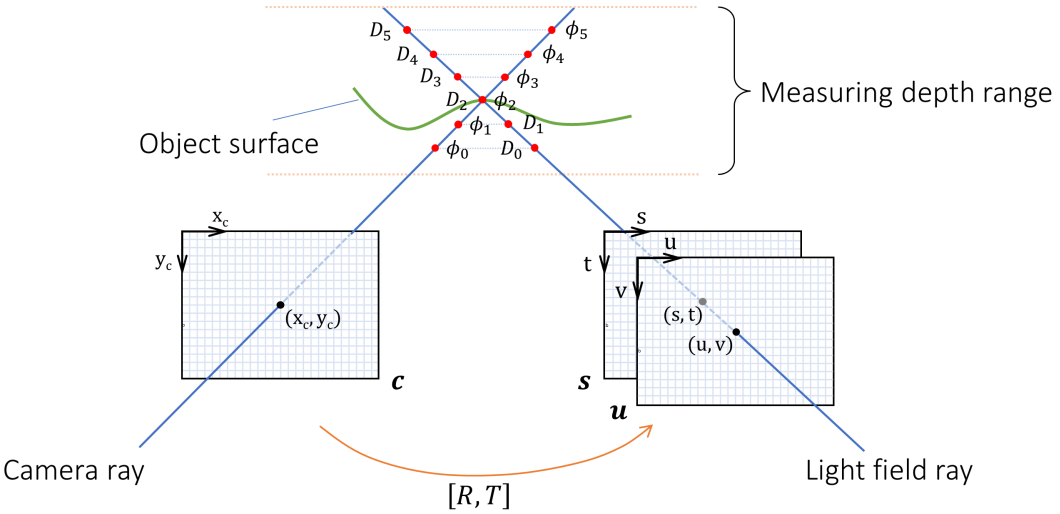

FIGURE 3. Light field assisted phase unwrapping model.

D belong to the world coordinate system and the light field coordinate system respectively measured in of mm. This transformation is no difference from the traditional coordinate transformation, represented by a rotation matrix R and a translation matrix T. The transformation of depth D can also be obtained by Eq.6, the mapping between unwrapped phase in imaging plane of camera $\phi_c^n(x, y)$ and absolute depth D corresponding to (u, v) can be established with the support of Eq.3, as showed in the following equation.

$$D = r_{31}X_c + r_{32}Y_c + r_{33}Z_c + t_3 = f_D(\phi) = \frac{1}{\sum_{n=1}^{N} e_n \phi_c^n(x, y)} \tag{7}$$

According to the above derivation, the conversion between D which characterizes the light field depth and the camera coordinate system depth characterization $\phi_c(x, y)$ has been completed, which means that the calibration work has also been completed and the wrapped phase can be expanded to the unwrapped phase according to the following theory without the need for additional timing code information.

As shown in Fig.3, different unwrapped phases correspond to different depths in the measuring depth range. The order k of the unwrapped phase is not irregular but changes within a certain range owing to the limits of the field of view and calibration space. Each wrapped phase has a candidate order sequence $[k_{min}, k_{max}]$, with in this sequence only one k_c is positive, and the other k are false interference items. The candidate order k_m, results in a series of candidate unwrapped phases $\phi_m(\phi_m = \phi_w + 2\pi k_m)$, of which only one is the correct unwrapped phase. According to Eq.7, each candidate phase ϕ_m corresponds to an absolute depth D in the light field coordinate. However, only one absolute depth D_c corresponds to the real object point in the field of view, which is equivalent to only one spatial point range focused when sampling. At the focus position, the light field and camera coordinate will correspond to the same point, and the correct order k_c can be determined by comparing the phase difference of the corresponding points in the two coordinate systems. The wrapped phase difference and the candidate order k_m are measured by the following equation:

$$\Delta\phi_w(\mathbf{s}) = \phi_w^{FPP}(x_c, y_c) - \phi_w^{LF}(\mathbf{u_{Dm}}, \mathbf{s}) \tag{8}$$

$$\Delta\Phi_w(k_m) = \frac{\sum_{\mathbf{s}}(\Delta\phi_w(\mathbf{s}) - \overline{\Delta\phi_w(\mathbf{s})})}{N - 1} \tag{9}$$

$\phi_w^{FPP}(x_c, y_c)$ is the wrapped phase in FPP, (x_c, y_c) refers to the point position of the wrapped phase position on the imaging surface of industrial camera. D_m corresponds to the absolute depth of the light field, which is connected to the unwrapped phase generated by the possible orders, and can be obtained by replacing $\phi_c(x, y)$ with ϕ_m on the basis of Eq.7 after calibration. $(\mathbf{u_{D_m}}, \mathbf{s})$ is the corresponding point position of the candidate phase after shearing is obtained according to Eq.4 in which $\mathbf{u_{D_m}} = (u_{D_m}, v_{D_m})$, $\mathbf{s} = (s, t)$ and $\phi_w^{LF}(\mathbf{u_{Dm}}, \mathbf{s})$ is the wrapped phase in the light field after shearing. Where $\Delta\Phi_w(k_m)$ denotes phase difference in the resampled wrapped phase-encoded field, $\mathbf{s}$ is a set of the angular coordinates associated with valid light rays and N is the number of selected angular coordinates. The valid light rays can be selected by using the modulation intensity with a given threshold. By minimizing $\Delta\Phi_w(k_m)$, the order can be determined by the following equation.

$$k_c = \arg\min_{k_m} \Delta\Phi_w(k_m) \tag{10}$$

Correspondingly, the correct fringe order k_c can be determined to obtain the unwrapped phase such that $\phi_c^{FPP} = \phi_w^{FPP} + 2\pi k_c$.

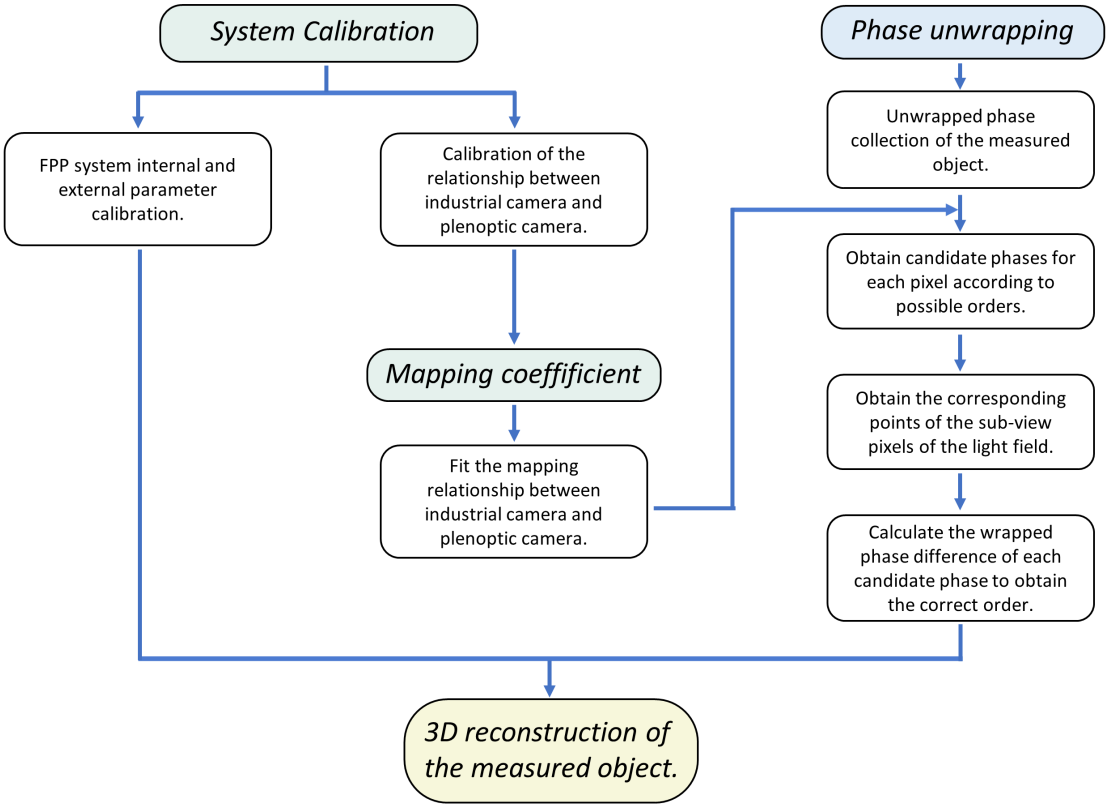

FIGURE 4. Two-step experiment flow chart: calibration and high-speed phase unwrapping.

III. EXPERIMENT

Based on the derivation in the previous section, we propose a method to use the light field to assist phase unwrapping and three-dimensional reconstruction. The method includes two steps: calibration and high-speed phase unwrapping. The overall process is shown in Fig.4.

In the calibration process, calibration is divided into two steps, including mapping the relationship between the industrial camera and the plenoptic camera, and the internal and external parameters of the FPP system. The calibration of the internal and external parameters of the FPP system adopts traditional methods to obtain subsequent three-dimensional information. The industrial camera and the plenoptic camera must be synchronized to collect the fringes to reduce errors caused by unstable factors. The calibration data is used to obtain the mapping coefficients, and this step must be completed before the phase unwrapping.

A. SYSTEM CALIBRATION

An industrial camera and a digital projector are used to form the FPP system, and the plenoptic camera is used to assist in obtaining light field (4-D) information. The overall system architecture is shown in Fig.5(a). The working distance was about 500mm. Light field images were decoded with spatial and angular resolutions of 434 $\times$ 625 pixels and 15 $\times$ 15 pixels, respectively.

Using the orthogonal unwrapped phase to establish a connection between the FPP system and the plenoptic camera to complete the system construction. Matching across the field of view is realized by means of calibrated camera orientation parameters and phase information extracted from ordinary and plenoptic camera views. Each pixel position on the camera can be mapped to the reference plane, and the phase can establish the connection between the camera plane and the light field imaging surface, that is, the same point in space is imaged in different positions on the light field and camera. The projector projects orthogonal sinusoidal fringes and Gray code on a smooth pure white plane target, and the plenoptic camera and industrial camera simultaneously sample different reference planes in the scene space at different depths. In the calibration process, the use of orthogonal stripes improves the stability of the mapping, and the use of Gray codes is also necessary to obtain the order information of the whole space in advance. When sampling phase for the measured object, only single-directional fringe patterns are projected, and Gray code patterns are no longer required. The data were acquired using static acquisition modes for the two phantoms at several different locations in relation to the longitudinal central axis of the field of view, that is, the center of the field of view. Obviously, the larger the number of selected reference surfaces, the more accurate the subsequent mapping coefficients will be. Considering the diminishing marginal

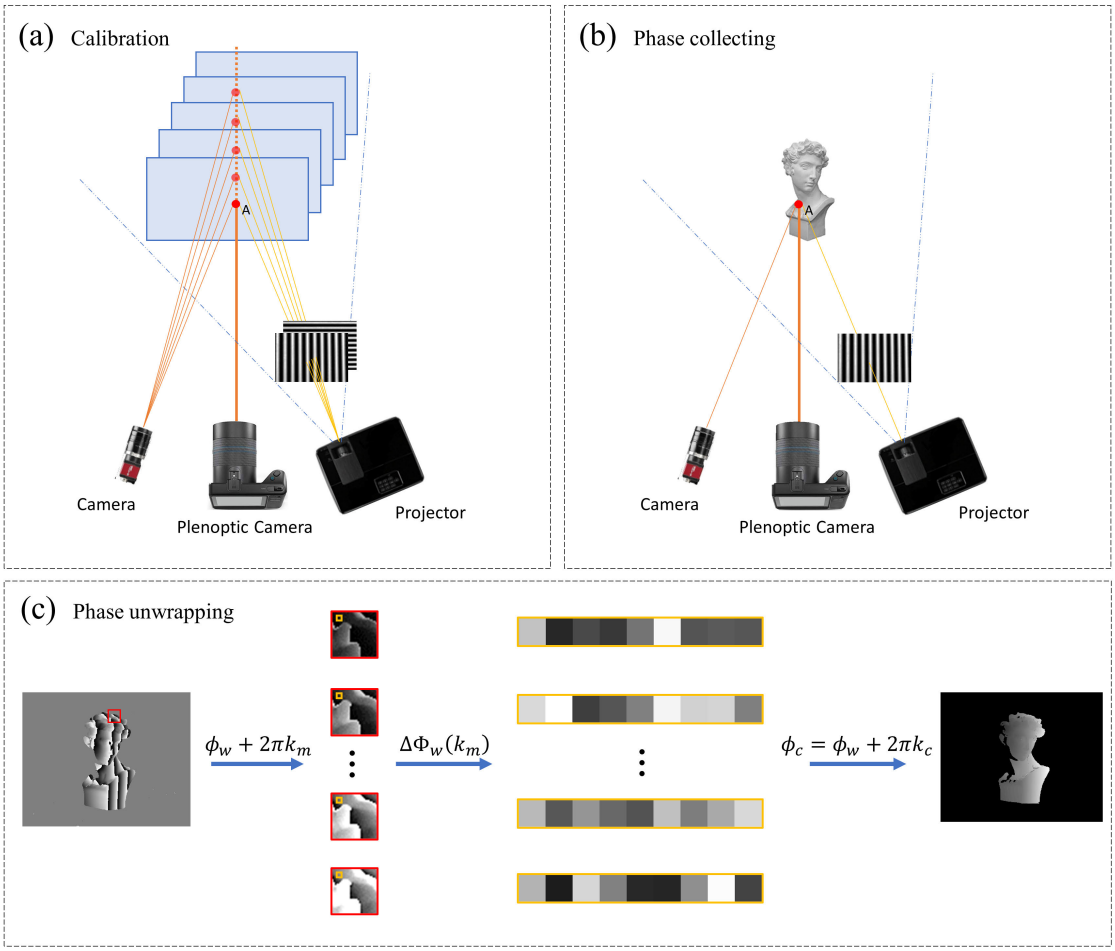

FIGURE 5. System calibration and phase unwrapping process. (a) Use orthogonal fringes to calibrate multi-depth planes (b) Use single-directional fringes to collect object topography information (c) Combine wrapped phase difference in different viewing angles of the possible order(k_m) to determine the correct order for phase unwrapping.

benefit, we have selected eleven reference surfaces, which are collected at intervals of one centimeter. After calibration, plenoptic data can be demultiplexed to a set of multi-view images that form a four-dimensional (4-D) data structure called the light field. In addition, the possible order of each point in the object space is determined by the depth of the object space during the calibration process, and will be used for subsequent phase expansion. Note that the calibration of the system is necessary and unique. After calibration, the relative position between the devices must not be changed. Once the stability of the system is destroyed, the mapping relationship obtained will no longer be accurate, and the orders can no longer be correctly unwrapped. The calibration of the FPP system is the same as the traditional method, using a planar target with dots to obtain the internal and external parameters of the system (Table 2) for subsequent 3D reconstruction.

B. MAPPING COEFFICIENT CALIBRATION

According to Eq.3, the absolute position in the imaging plane of camera is obtained with the help of the absolute phase unwrapping by the Gray code at different reference planes. Through the derivation of the second section, we establish a mapping from the imaging surface of the industrial camera to the sub-view of the plenoptic camera by the medium of depth. In the measured space, for each pixel, the unwrapped phase represents the depth information, which is a stable and effective medium in the above relationship. Taking the unwrapped phase as the landmark point, combined with the unwrapped phase of different depths obtained by calibration, the pixel-to-pixel mapping relationship between the industrial camera and the plenoptic camera is established. The pixel position of the imaging plane of the industrial camera (x_c, y_c) and the plenoptic camera (u, v) are determined simultaneously with regard to a point in space with a specific phase. In different viewing angles of the light field, the pixel positions of the imaging surface of the plenoptic camera are fitted with the same phase point of the undetermined pixel on the imaging surface of the industrial camera($u = \frac{1}{\sum_{n=1}^{N} A_n \phi_c^n(x_c, y_c)}, v = \frac{1}{\sum_{n=1}^{N} B_n \phi_c^n(x_c, y_c)}$). Thus, given the arbitrary phase ϕ on the

TABLE 1. FPP system parameters.

	projector	camera
f_x, f_y(pixel)	1968.1, 1963.4	2323.0, 2322.5
x_0, y_0(pixel)	639.7285, 758.4176	642.49.1, 489.6877
k	0.00110, -0.2327, -0.0042, -0.0014, 0	-0.0908, 0.3280, -0.0001, -0.0018, 0
r_s	0.1841, 0.4834, 0.0547	
t_s	-277.632, -37.2132, 190.9049	

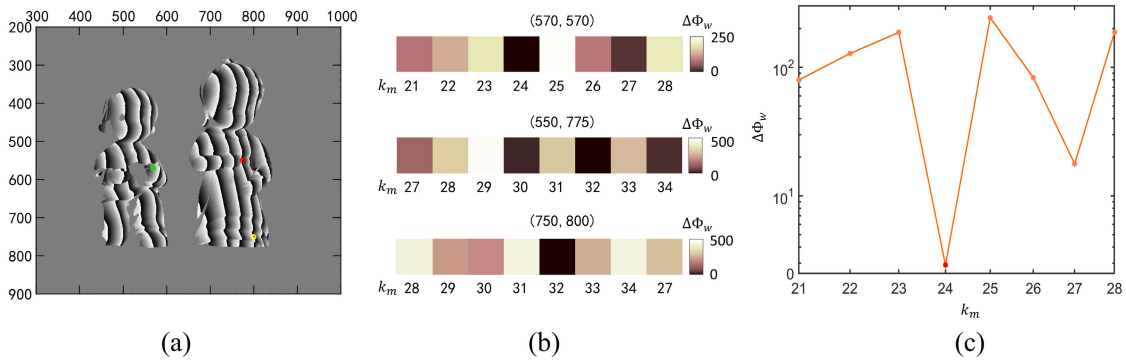

FIGURE 6. The unwrapped phase difference of possible orders to determine the correct k_c. (a) Wrapped phase and special points, the green marking point (570, 570) is on the hand of the doll, the red marking point (550, 775) is on the hand of the doll and the discontinuous edge of the order, the yellow marking points (750, 800) is at the discontinuous edge of the order of the doll skirt (b)Wrapped phase difference $\Delta\phi_W$ of possible orders at special points (c)The wrapped phase difference of possible order at point (570, 570).

imaging surface of the industrial camera, the coordinates of the imaging surface of the plenoptic camera can be obtained. The mapping coefficients A and B mentioned are the mapping coefficients from the imaging surface of the industrial camera to the imaging surface of the plenoptic camera. The mapping includes coordinate transformation and lens distortion of the projector, and even some errors that not able to be analyze are included, and avoiding the correction of distortion caused by the complex structure of the plenoptic camera. Different light field sub-view angles have a unique set of corresponding mapping coefficients A and B. The mapping coefficients of the required sub-view angles must be obtained, and then the order can be determined according to the phase consistency. Selection of the number of sub-views is controllable, and horizontal selection is better than vertical selection. We select 9 views in the center of the row where the center sub-view is located. The greater the number of selected sub-views, the more mapping coefficients that need to be fitted, and the higher the accuracy of the expansion level, but it becomes more time-consuming. The greater the parallax between the sub-views, the more beneficial it is for level determination, so interval selection of the sub-views is a good solution, but the most marginal views should be avoided.

C. PHASE UNWRAPPING

In order to reduce the sampling time, only the horizontal sinusoidal fringes are projected, and the wrapped phase of the object can be obtained with the help of Eq.2 as showing in Fig.5(b). The possible order of each pixel obtained in 3.1 is added to the wrapped phase to obtain the candidate phase of the object point. With the aid of the second of calibration step, the corresponding points of each light field viewing angle related to the imaging surface of the industrial camera can be obtained as shown in Fig.5(c). The pixel position of each sub-view is obtained with the support of the candidate phase and the mapping coefficient of each sub-view. The candidate phase which corresponding to the smallest sum of the wrapped phase difference between each sub-view pixel and the original pixel of the industrial camera is the correct phase. Fig.6(b) shows the sum of the wrapped phase errors($\Delta\Phi_w(k_m)$) of different levels. Only under the correct order, which means when the corresponding depth is correct, is the sum of the wrapped phase errors extremely small.

The non-corresponding order will produce a large $\Delta\Phi_w(k_m)$, which is of a different order of magnitude from $\Delta\Phi_w(k_c)$, which largely avoids the confusion of the order and provides a robust solution for our method. As showing in Fig.6(c), the correct unwrapped phase can be determined by comparing $\Delta\Phi_w(k_m)$ of all the candidate phase points and the wrap phase obtained by the FPP system. In the continuous range, the continuous order of blockbusters k_c can be obtained, and level errors do not occur easily. At the discontinuous edge of order and where the object is delicate, the error of order expansion is occurs easily, but our method solves this problem effectively. We show three special points of different order $\Delta\Phi_w(k_m)$, (570, 570) and (575, 775) in the hand of the doll, while (575, 775) and (750, 800) are at

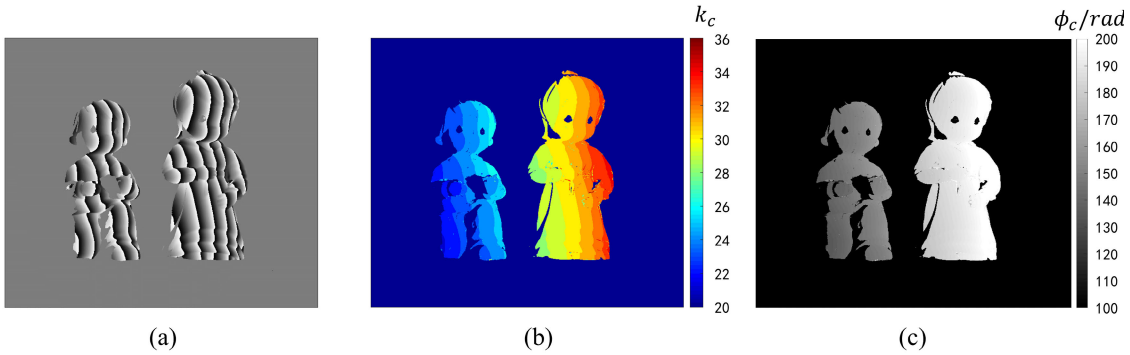

FIGURE 7. The absolute phase unwrapping for the measured scene. (a)Unwrapped phase (b)The correct fringe orders k_c (c)The unwrapped phase ϕ_c.

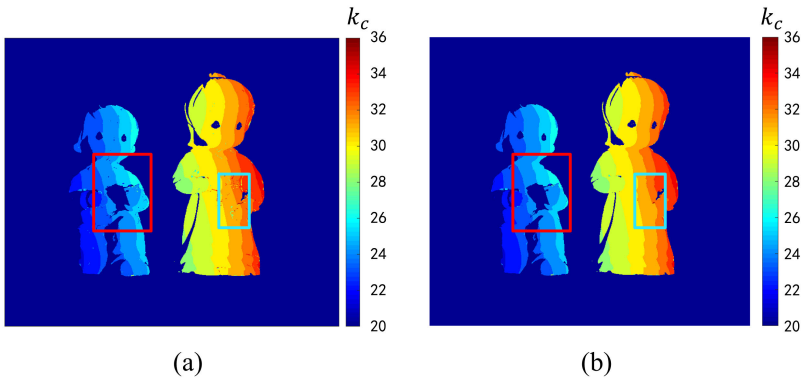

FIGURE 8. (a) The fringe orders k_c before compensation (b) The fringe orders k_c after compensation.

discontinuities in the order. In Fig.6(b), the smallest $\Delta\Phi_w(k_m)$ corresponds to the correct $\Delta\Phi_w(k_c)$, the errors of other orders are very different from the correct order, which makes our phase unwrapping stable and accurate. According to the above process, all other pixels can be processed to determine the correct fringe order as shown in the Fig.7(b).

Since the correct order is obtained, the absolute phase after phase unwrapping is shown in Fig.7(c), which has good continuity and can be used for 3D reconstruction. We studied the robustness and stability of the method, and conducted experiments on objects of different sizes and different field of view ranges, which proved the effectiveness of the method. Since the plenoptic camera is an ultra-short epipolar light field acquisition device, very few pixels lack accurate corresponding points and cannot be fitted. We consider that the angle between the optical axis of the equipment, the flaws on the target, the field of view limitation, and the insufficient algorithm will all cause this phenomenon. Therefore, individual pixel cannot be unwrapped, and algorithms must be combined with the surrounding levels to compensate. In the case that the order is correct in a wide range, the order is determined by comparing whether the phase difference between the missing point and the surrounding pixels is greater than the threshold. The orders after algorithm compensation are shown in Fig.8. In the red and blue boxes, most of the grade information of the missing points is correctly compensated.

Through the rapid phase unwrapping method in this article, additional temporal coding will no longer be needed to reduce the sampling time. The fringe pattern sample of sequential coding is determined by the resolution of the projector and the width of the projected fringe. The thinner the fringe width is, the more samples of the fringe pattern are needed, which leads to a longer collection time. The resolution of the projector used is 1280×800, the fringe width is 12, and the number of phase steps is 12,8 sheets of grey code is demanded corresponding. The proposed method can save 40% of the time, and 66.7% of the time can be saved if the four-step phase shift is used. The lower the number of phase steps, the short the acquisition time. However an increase in the number of phase steps can effectively suppress the gamma effect. With the help of previous work and the correct order k_c, the 3D reconstruction work can be completed as shown in Fig.9.

Regarding the projector as the inverse of the camera, with the support of the FPP system parameters obtained in Section 3.1, the monocular system maintains high-precision object reconstruction. As shown in Fig.10, we measured the reconstruction accuracy of the experimental system. The results of our error evaluation of the system using the standard

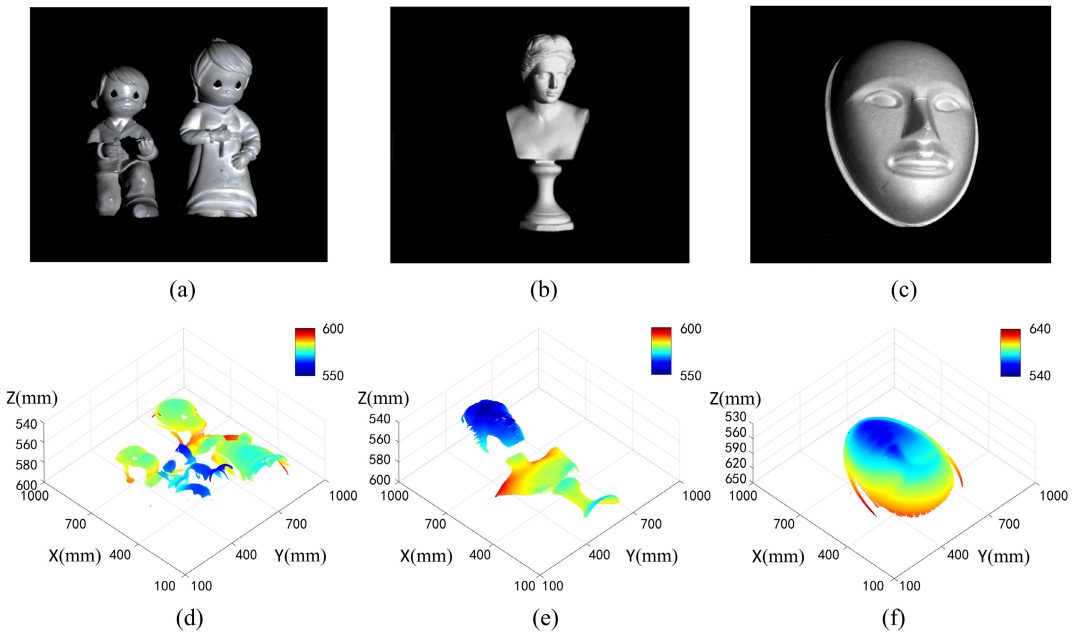

FIGURE 9. 3D model reconstructed after phase unwrapping. (a), (b) and (c) are dolls, sculptures and masks, (d), (e) and (f) are their 3D reconstruction models respectively.

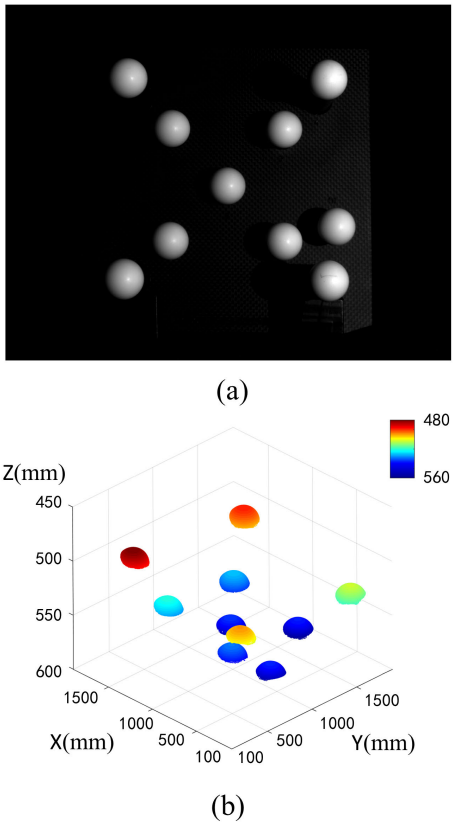

FIGURE 10. 3D model reconstructed of standard sphere. (a)Standard spherical surface to be measured (b)3D reconstruction model.

sphere and the distance between the center of the sphere are shown in Table 2, which shows that the system maintains the accuracy of FPP.

TABLE 2. Data error of spherical fitting and spherical center distance fitting (mm).

	Spherical fitting errors			Spherical center distance fitting errors	
	Average radius	MAX	STD	MAX	STD
1	25.34747	0.1132	0.035387	0.10645	0.042462
2	25.3566	0.1211	0.040391	0.111719	0.044053

IV. CONCLUSION

Our research aims to provide an effective method for phase unwrapping, which uses less phase acquisition time to obtain stable and robust results. We determine the correct fringe order by checking the consistency of the wrapping phases of the FPP system and the assisted light field in different spatial positions corresponding to a series of candidate unwrapped phase points, thus successfully realizing the phase unwrapping of the FPP system. The proposed method uses, but is not limited to, a plenoptic camera, and can be extended to other light field imaging devices. Experiments show that this method has met our expectations, has a good phase unwrapping effect, and can be used for reconstruction. The particular strength of this study is its ability to eliminate the limitation on the number of micro lenses that can be used, which maintains the resolution and reduces additional coding time. In the future, we will conduct more in-depth exploration on the reduction of acquisition time, combined with the effective phase unwrapping method proposed in this paper to achieve high-speed real-time 3D reconstruction.

DISCLOSURES

The authors declare no conflicts of interest.

REFERENCES

[1] C. Zuo, Q. Chen, G. Gu, S. Feng, and F. Feng, "High-speed three-dimensional profilometry for multiple objects with complex shapes," *Opt. Exp.*, vol. 20, no. 17, p. 19493, 2012.

[2] S. Zhang, D. Van Der Weide, and J. Oliver, "Superfast phase-shifting method for 3-D shape measurement," *Opt. Exp.*, vol. 18, no. 9, p. 9684, 2010.
[3] C. Zuo, S. Feng, L. Huang, T. Tao, W. Yin, and Q. Chen, "Phase shifting algorithms for fringe projection profilometry: A review," *Opt. Lasers Eng.*, vol. 109, pp. 23–59, Oct. 2018.
[4] J. Xu, S. Liu, A. Wan, B. Gao, Q. Yi, D. Zhao, R. Luo, and K. Chen, "An absolute phase technique for 3D profile measurement using four-step structured light pattern," *Opt. Lasers Eng.*, vol. 50, no. 9, pp. 1274–1280, Sep. 2012.
[5] Z. Zhang, S. Huang, Y. Xu, C. Chen, Y. Zhao, N. Gao, and Y. Xiao, "3D palmprint and hand imaging system based on full-field composite color sinusoidal fringe projection technique," *Appl. Opt.*, vol. 52, no. 25, pp. 6138–6145, Sep. 2013.
[6] R. M. Goldstein, H. A. Zebker, and C. L. Werner, "Satellite radar interferometry: Two-dimensional phase unwrapping," *Radio Sci.*, vol. 23, no. 4, pp. 713–720, Jul. 1988.
[7] X. Su and W. Chen, "Reliability-guided phase unwrapping algorithm: A review," *Opt. Lasers Eng.*, vol. 42, no. 3, pp. 245–261, Sep. 2004.
[8] T. J. Flynn, "Two-dimensional phase unwrapping with minimum weighted discontinuity," *J. Opt. Soc. Amer. A, Opt. Image Sci.*, vol. 14, no. 10, pp. 2692–2701, 1997.
[9] Z. Zhang, Z. Jing, Z. Wang, and D. Kuang, "Comparison of Fourier transform, windowed Fourier transform, and wavelet transform methods for phase calculation at discontinuities in fringe projection profilometry," *Opt. Lasers Eng.*, vol. 50, no. 8, pp. 1152–1160, Aug. 2012.
[10] C. Zuo, L. Huang, M. Zhang, Q. Chen, and A. Asundi, "Temporal phase unwrapping algorithms for fringe projection profilometry: A comparative review," *Opt. Lasers Eng.*, vol. 85, pp. 84–103, Oct. 2016.
[11] J. M. Huntley and H. Saldner, "Temporal phase-unwrapping algorithm for automated interferogram analysis," *Appl. Opt.*, vol. 32, no. 17, p. 3047, 1993.
[12] V. I. Gushov and Y. N. Solodkin, "Automatic processing of fringe patterns in integer interferometers," *Opt. Lasers Eng.*, vol. 14, nos. 4–5, pp. 311–324, 1991.
[13] Y.-Y. Cheng and J. C. Wyant, "Two-wavelength phase shifting interferometry," *Appl. Opt.*, vol. 23, no. 24, p. 4539, 1984.
[14] X. Peng, Z. Yang, and H. Niu, "Multi-resolution reconstruction of 3-D image with modified temporal unwrapping algorithm," *Opt. Commun.*, vol. 224, nos. 1–3, pp. 35–44, Aug. 2003.
[15] G. Sansoni, M. Carocci, and R. Rodella, "Three-dimensional vision based on a combination of gray-code and phase-shift light projection: Analysis and compensation of the systematic errors," *Appl. Opt.*, vol. 38, no. 31, pp. 6565–6573, Nov. 1999.
[16] J. Xu, B. Gao, J. Han, J. Zhao, S. Liu, Q. Yi, Z. Zhao, H. Yin, and K. Chen, "Realtime 3D profile measurement by using the composite pattern based on the binary stripe pattern," *Opt. Laser Technol.*, vol. 44, no. 3, pp. 587–593, Apr. 2012.
[17] R. Ishiyama, S. Sakamoto, J. Tajima, T. Okatani, and K. Deguchi, "Absolute phase measurements using geometric constraints between multiple cameras and projectors," *Appl. Opt.*, vol. 46, no. 17, pp. 3528–3538, 2007.
[18] Z. Li, K. Zhong, Y. F. Li, X. Zhou, and Y. Shi, "Multiview phase shifting: A full-resolution and high-speed 3d measurement framework for arbitrary shape dynamic objects," *Opt. Lett.*, vol. 38, no. 9, pp. 1389–1391, 2013.
[19] C. Bruer-Burchardt, C. Munkelt, M. Heinze, P. Kühmstedt, and G. Notni, "Using geometric constraints to solve the point correspondence problem in fringe projection based 3D measuring systems," in *Image Analysis and Processing—ICIAP* (Lecture Notes in Computer Science). Washington, DC, USA: The Optical Society, 2011.
[20] A. G. Orth and K. B. Crozier, "Light field moment imaging," *Opt. Lett.*, vol. 38, no. 15, pp. 2666–2668, 2013.
[21] T. Tao, Q. Chen, Y. Zhang, Y. Hu, J. Da, and C. Zuo, "Multi-view phase unwrapping with composite fringe patterns," in *Proc. Int. Conf. Opt. Photon. Eng. (icOPEN)*, Feb. 2017, Art. no. 1025017.
[22] B. Wilburn, "High-performance imaging with large camera arrays," in *Proc. ACM SIGGRAPH Courses - SIGGRAPH*, 2006, pp. 42–113.
[23] A. Veeraraghavan, R. Raskar, A. Agrawal, A. Mohan, and J. Tumblin, "Dappled photography: Mask enhanced cameras for heterodyned light fields and coded aperture," *ACM Trans. Graph.*, vol. 26, no. 3, p. 69, 2007.
[24] K. Atanassov, S. Goma, V. Ramachandra, and T. Georgiev, "Content-based depth estimation in focused plenoptic camera," *Proc. SPIE*, vol. 7864, Jan. 2011, Art. no. 78640G.
[25] C. Kim, H. Zimmer, Y. Pritch, A. Sorkine-Hornung, and M. Gross, "Scene reconstruction from high spatio-angular resolution light fields," *ACM Trans. Graph.*, 2013.
[26] M. W. Tao, S. Hadap, J. Malik, and R. Ramamoorthi, "Depth from combining defocus and correspondence using light-field cameras," in *Proc. IEEE Int. Conf. Comput. Vis.*, Dec. 2013, pp. 673–680.
[27] M. W. Tao, P. P. Srinivasan, S. Hadap, S. Rusinkiewicz, J. Malik, and R. Ramamoorthi, "Shape estimation from shading, defocus, and correspondence using light-field angular coherence," *IEEE Trans. Pattern Anal. Mach. Intell.*, vol. 39, no. 3, pp. 546–560, Mar. 2017.
[28] Y. Zhang, H. Lv, Y. Liu, H. Wang, X. Wang, Q. Huang, X. Xiang, and Q. Dai, "Light-field depth estimation via epipolar plane image analysis and locally linear embedding," *IEEE Trans. Circuits Syst. Video Technol.*, vol. 27, no. 4, pp. 739–747, Apr. 2017.
[29] C. Hahne, A. Aggoun, V. Velisavljevic, S. Fiebig, and M. Pesch, "Refocusing distance of a standard plenoptic camera," *Opt. Exp.*, vol. 24, no. 19, p. 21521, 2016.
[30] Y. Chen, X. Jin, and Q. Dai, "Distance measurement based on light field geometry and ray tracing," *Opt. Exp.*, vol. 25, no. 1, p. 59, 2017.
[31] Z. Cai, X. Liu, Z. Chen, Q. Tang, B. Z. Gao, G. Pedrini, W. Osten, and X. Peng, "Light-field-based absolute phase unwrapping," *Opt. Lett.*, vol. 43, no. 23, p. 5717, 2018.
[32] Z. Cai, X. Liu, X. Peng, Y. Yin, A. Li, J. Wu, and B. Z. Gao, "Structured light field 3D imaging," *Opt. Exp.*, vol. 24, no. 18, 2016, Art. no. 20324.
[33] Z. Cai, X. Liu, X. Peng, and B. Z. Gao, "Ray calibration and phase mapping for structured-light-field 3D reconstruction," *Opt. Exp.*, vol. 26, no. 6, p. 7598, 2018.
[34] Z. Cai, X. Liu, Q. Tang, X. Peng, and B. Z. Gao, "Light field 3D measurement using unfocused plenoptic cameras," *Opt. Lett.*, vol. 43, no. 15, p. 3746, 2018.
[35] Z. Cai, X. Liu, A. Li, Q. Tang, X. Peng, and B. Z. Gao, "Phase-3D mapping method developed from back-projection stereovision model for fringe projection profilometry," *Opt. Exp.*, vol. 25, no. 2, pp. 1262–1277, 2017.

ZIWEI WANG was born in Fujian, China, in 1997. She received the B.S. degree in applied physics from Henan Polytechnic University, Jiaozuo, Henan, China, in 2019. She is currently pursuing the M.S. degree with Shenzhen University. Her research interests include the optical metrology, light field, and Bessel light illumination.

YANG YANG was born in Jinzhong, Shanxi, China, in 1991. He received the B.S. degree from the North University of China, in 2014, and the M.S. degree from Shenzhen University, in 2018, where he is currently pursuing the Ph.D. degree. His research interests include the optical metrology and 3D optical digital imaging and modeling.

XIAOLI LIU was born in Hebei, China. He received the B.S., M.S., and Ph.D. degrees from Tianjin University. Since 2008, he has been working with Shenzhen University, where he became an Associate Professor, in 2018. He has published more than 70 papers in important academic journals and conferences and has applied for 30 patents. His research interests include 3D optical digital imaging and modeling, machine vision, optical detection, optical field imaging, and computer graphics.

YUPEI MIAO was born in Shenzhen, Guangdong, China, in 1998. He received the B.S. degree from Shenzhen University, China, in 2019, where he is currently pursuing the M.S. degree. His research interests include the 3D optical digital imaging and 3D machine vision.

QUANYAO HOU was born in Zhongshan, Guangdong, China, in 1996. He received the B.S. degree from Shenzhen University, in 2019, where he is currently pursuing the M.S. degree. His research interests include the light field deep learning and 3D optical digital imaging.

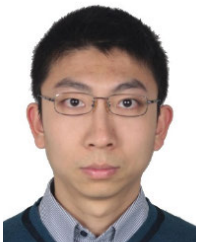

YONGKAI YIN received the B.E. degree in electronics science and technology from Tianjin University, in 2006, the M.E. degree in physical electronics from Shenzhen University, in 2009, and the Ph.D. degree in instrument science and technology from Tianjin University, in 2012. He is currently an Associate Professor with the School of Information Science and Engineering, Shandong University, China. His research interests include optical 3D imaging and metrology, and computational imaging.

ZEWEI CAI received the B.S. and M.S. degrees in measurement and control technology and instrument and the Ph.D. degree in optical engineering from Shenzhen University, China, in 2012 and 2017, respectively. His research interests include optical three-dimensional imaging and metrology.

QIJIAN TANG received the B.S., M.S., and Ph.D. degrees from Tianjin University. Since 2018, he has been a Lecturer with Shenzhen University. His research interests include Fourier tomography, and 3D optical digital imaging and modeling.

XIANG PENG received the B.S., M.S., and Ph.D. degrees from Tianjin University, in 1981, 1984, and 1989, respectively, all in optical engineering. In 1984, he was with Tianjin University, as an Assistant Professor. From 1990 to 1992, he worked with the Institute of Applied Optics, University of Stuttgart, as an Alexander von Humboldt Fellow. He was with Tianjin University, as an Associate Professor, in 1996, and a Full Professor, in 1998. Since 2003, he has been a Full Professor with Shenzhen University. He has authored and coauthored over 100 refereed journal articles and holds over 20 patents. His current research interests include optical imaging, optical metrology, and optical security.